Available online at www.sciencedirect.com
ScienceDirect
Acta Materialia 58 (2010) 5547–5557
Acta MATERIALIA
www.elsevier.com/locate/actamat

Activated states for cross-slip at screw dislocation intersections in face-centered cubic nickel and copper via atomistic simulation

S.I. Rao [a,*], D.M. Dimiduk [b], J.A. El-Awady [c], T.A. Parthasarathy [a], M.D. Uchic [b], C. Woodward [b]

[a] UES Inc., 4401 Dayton-Xenia Road, Dayton, OH 45432-1894, USA
[b] Air Force Research Laboratory, Materials and Manufacturing Directorate, AFRL/MLLM Wright-Patterson AFB, OH 45433-7817, USA
[c] UTC, Dayton, OH 45432, USA

Received 1 March 2010; received in revised form 13 May 2010; accepted 2 June 2010
Available online 23 July 2010

Abstract

We extend our recent simulation studies where a screw dislocation in face-centered cubic (fcc) Ni was found to spontaneously attain a low energy partially cross-slipped configuration upon intersecting a forest dislocation. Using atomistic (molecular statics) simulations with embedded atom potentials, we evaluated the activation barrier for a dislocation to transform from fully residing on the glide plane to fully residing on a cross-slip plane intersecting a forest dislocation in both Ni and Cu. The activation energies were obtained by determining equilibrium configurations (energies) when variable pure tensile or compressive stresses were applied along the [1 1 1] direction on the partially cross-slipped state. We show that the activation energy is a factor of 2–5 lower than that for cross-slip in isolation via the Escaig process. The cross-slip activation energies obtained at the intersection in Cu were in reasonable accord with the experimentally determined cross-slip activation energy for Cu. Further, the activation barrier for cross-slip at these intersections was shown to be linearly proportional to $(d/\mathbf{b})[\ln(\sqrt{3}d/\mathbf{b})]^{1/2}$, as in the Escaig process, where d is the Shockley partial dislocation spacing and $\mathbf{b}$ is the Burgers vector of the screw dislocation. These results suggest that cross-slip should be preferentially observed at selected screw dislocation intersections in fcc materials.

Keywords: Cross-slip; Activation analysis; Atomistic simulations; Nickel; Escaig stresses

1. Introduction

There is increasing recognition of the need to incorporate physics-based models of deformation in the design of structural components. While models for predicting yield strength and creep behavior are beginning to incorporate significant physics, models for fatigue and ultimate strength remain mostly empirical. This is because strain hardening and fatigue resistance are highly influenced by dislocation micromechanisms, for example cross-slip, and including physics-based cross-slip processes in mesoscale simulations (e.g. dislocation dynamics) has been difficult. The early work of Escaig remains the most widely cited and used model for cross-slip [1–4], however, this model poses several difficulties with respect to quantitative simulations. The model is highly sensitive to choice of parameters that have thus far been difficult to obtain. For example, the constriction width required for cross-slip is unknown but significantly influences the enthalpy of the cross-slip process [5]. This difficulty has led to an ad hoc postulate that obstacles always exist in materials which enable sufficient dislocation core constriction under stress, thereby ensuring cross-slip [1]. Aside from being a presumption, this forces cross-slip models (particularly for single crystals) to make arbitrary assumptions about the dislocation obstacle spacing. Advances in atomistic simulations make it possible to gain insights into the cross-slip

* Corresponding author. Tel.: +1 9372551318; fax: +1 9372553007.
E-mail address: satish.rao@wpafb.af.mil (S.I. Rao).

1359-6454/$36.00 © 2010 Acta Materialia Inc. Published by Elsevier Ltd. All rights reserved.
doi:10.1016/j.actamat.2010.06.005

Report Documentation Page

Form Approved
OMB No. 0704-0188

1. REPORT DATE	2. REPORT TYPE	3. DATES COVERED
23 JUL 2010		**00-00-2010 to 00-00-2010**

4. TITLE AND SUBTITLE
Activated states for cross-slip at screw dislocation intersections in face-centered cubic nickel and copper via atomistic simulation

5a. CONTRACT NUMBER
5b. GRANT NUMBER
5c. PROGRAM ELEMENT NUMBER

6. AUTHOR(S)

5d. PROJECT NUMBER
5e. TASK NUMBER
5f. WORK UNIT NUMBER

7. PERFORMING ORGANIZATION NAME(S) AND ADDRESS(ES)
Air Force Research Laboratory,Materials and Manufacturing Directorate, AFRL/MLLM,Wright-Patterson AFB,OH,45433-7817

8. PERFORMING ORGANIZATION REPORT NUMBER

9. SPONSORING/MONITORING AGENCY NAME(S) AND ADDRESS(ES)

10. SPONSOR/MONITOR'S ACRONYM(S)
11. SPONSOR/MONITOR'S REPORT NUMBER(S)

12. DISTRIBUTION/AVAILABILITY STATEMENT
Approved for public release; distribution unlimited

13. SUPPLEMENTARY NOTES

14. ABSTRACT

We extend our recent simulation studies where a screw dislocation in face-centered cubic (fcc) Ni was found to spontaneously attain a low energy partially cross-slipped configuration upon intersecting a forest dislocation. Using atomistic (molecular statics) simulations with embedded atom potentials, we evaluated the activation barrier for a dislocation to transform from fully residing on the glide plane to fully residing on a cross-slip plane intersecting a forest dislocation in both Ni and Cu. The activation energies were obtained by determining equilibrium configurations (energies) when variable pure tensile or compressive stresses were applied along the [1 1 1] direction on the partially cross-slipped state. We show that the activation energy is a factor of 2?5 lower than that for cross-slip in isolation via the Escaig process. The cross-slip activation energies obtained at the intersection in Cu were in reasonable accord with the experimentally determined cross-slip activation energy for Cu. Further, the activation barrier for cross-slip at these intersections was shown to be linearly proportional to (d/b)[ln(ffiffiffi 3 p d/b)]1/2, as in the Escaig process, where d is the Shockley partial dislocation spacing and b is the Burgers vector of the screw dislocation. These results suggest that cross-slip should be preferentially observed at selected screw dislocation intersections in fcc materials.

15. SUBJECT TERMS

16. SECURITY CLASSIFICATION OF:			17. LIMITATION OF ABSTRACT	18. NUMBER OF PAGES	19a. NAME OF RESPONSIBLE PERSON
a. REPORT	b. ABSTRACT	c. THIS PAGE			
unclassified	**unclassified**	**unclassified**	**Same as Report (SAR)**	**11**	

process and may serve to inform mesoscale simulations to accurately capture the atomic level physics of that dislocation process. Such an insight was realized in our recent work [6], where the possibility of cross-slip at dislocation–dislocation intersections was selectively examined using large-scale atomistic simulations that contained more than one dislocation. A glide dislocation that intersects a pair of forest dislocations was modeled and several conditions were shown to exist where cross-slip can nucleate easily. This provides a better physical basis for cross-slip and the means to incorporate realistic cross-slip evolution in larger scale, discrete dislocation dynamics simulations. Further, this may lead to a realistic statistical representation of cross-slip during monotonic or cyclic deformation. However, this prior work did not explore the size and nature of the activation barrier for dislocation transformation at intersections.

In this work, we show that a finite energy barrier exists for cross-slip at an intersection, but that it is much smaller than that obtained from analyses of the Escaig process. Molecular statics simulations were used to determine the saddle point configuration and activation energy by using an applied stress to change the extent of partial dislocation cross-slip. The applied stresses were compressive or tensile along the [1 1 1] direction on the partially cross-slipped dislocation structures obtained in a prior work [6]. The screw character dislocation under study had a $1/2[1\,\bar{1}\,0]$ Burgers vector and the intersecting dislocation had a $1/2[\bar{1}\,0\,1]$ Burgers vector on the $(1\,\bar{1}\,1)$ plane and a 120° line orientation of $[0\,-1\,-1]$ (see Fig. 1). Section 2 describes the simulation technique and the interatomic potentials. Section 3 presents a review of the core structures obtained for this specific intersection [6] in Ni, as well as core structures obtained from atomistic simulations for this specific intersection in Cu, the effect of applied stresses along the [1 1 1] direction on the partially cross-slipped core structure, identification of the saddle point configuration and a determination of the energies of the activated state for cross-slip. Finally, Sections 4 and 5 give a discussion and summary of the results, respectively.

2. Simulation technique

The atomistic simulations described here employed the 3-dimensional (3D) parallel molecular dynamics code LAAMPS [7], developed at Sandia National Laboratory. A schematic of the simulation cell used in the atomistic simulations is given in Fig. 1. The simulation cell was a rectangular parallelepiped having the x-axis oriented along $[1\,\bar{1}\,0]$, the y-axis along $[1\,1\,\bar{2}]$ and the z-axis along [1 1 1]. The dimensions of the simulation cell were 62.0 nm along the x-axis and 31.5 nm along both the y- and z-axes, corresponding to a simulation cell of 5,405,160 atoms. The partially cross-slipped core structures obtained for the screw ($1/2[\bar{1}\,1\,0]$ Burgers vector)–120° ($1/2[\bar{1}\,0\,1]$ Burgers vector, $[0\,\bar{1}\,\bar{1}]$ line direction) intersection in Rao et al. [6], as well as for Cu, were subjected to uniform compressive or tensile stresses applied along the [1 1 1] direction. Under such a state of stress there were no resolved shear stresses acting along the Burgers vector direction for either the screw or the 120° dislocation. Also, there were no applied Escaig stresses acting on the edge components of the screw character dislocation on the (1 1 1) glide plane. However, there were Escaig stresses acting on the edge components of the screw dislocation on the cross-slip $(1\,1\,\bar{1})$ plane, as well as the forest dislocation on the $(1\,\bar{1}\,1)$ plane. Fixed

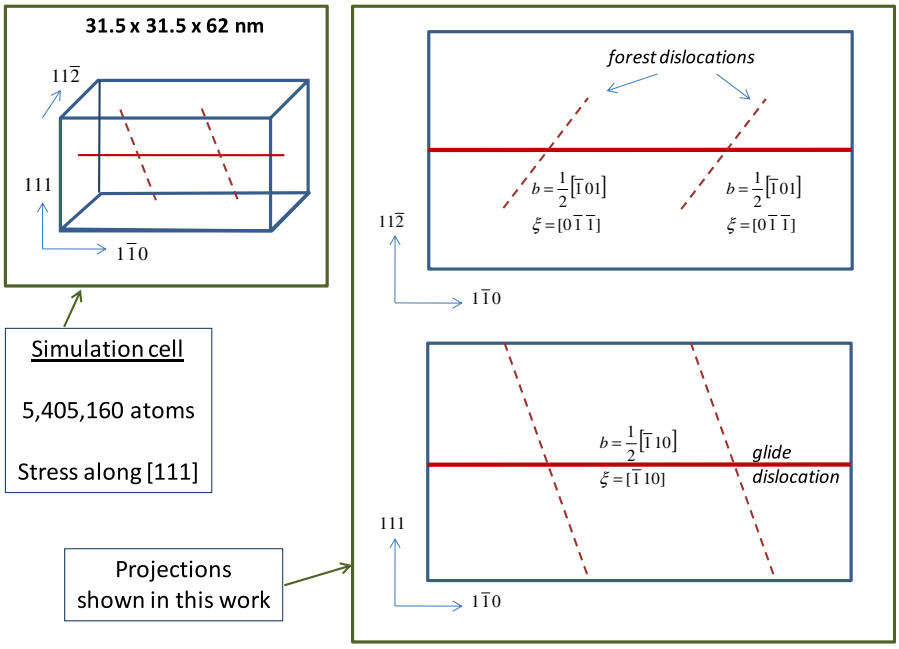

Fig. 1. A schematic of the simulation cell used in the atomistic simulations described in this manuscript.

boundary conditions were applied along all three directions and energy minimization was performed using the conjugate gradient technique. Such results were analyzed to obtain the energy differences between the fully on glide plane core structure, fully on cross-slip plane core structure and the activated structures for this intersection.

The approach used to obtain activation energies for transformation from one core structure to another was as follows. As the stress was varied, the relative magnitudes of Escaig stresses on the glide plane and cross-slip plane changed, thus affecting a variation in the length of the partially cross-slipped region of the screw character dislocation. Note that stabilizing each configuration required manipulation of the stresses before, after and at the inflection point in the energy–distance coordinate. By releasing the stress from the stabilized state, the configuration was allowed to "fall" towards either side of the saddle point configuration. This process allowed the identification of the saddle point configuration (within the energy error of the technique). Once identified, the absolute energy of this configuration without the applied stress was calculated by freezing a small volume of atoms near the core transformation region and then minimizing the energy of all other atoms in the cell. This gave an upper bound for the energy of the saddle point. The activation energy was obtained by subtracting the energy of the fully glide plane spread core configuration from that of the saddle point configuration. The primary error in this calculation arose from the fact that an arbitrary number of atoms were kept fixed while obtaining the energy of the saddle point configuration without applied stress and was estimated to be of the order of 0.2 eV.

2.1. Interatomic potential

The embedded atom potentials used for the simulations were those developed for face-centered cubic (fcc) Ni by Angelo, Moody and Baskes [8] based on the Voter and Chen format (Angelo), as well as the two Ni potentials developed based on the Voter and Chen format which Rao et al. used in their bulk cross-slip simulations, vni and vnih [9]. The embedded atom potential used for simulations of Cu was that developed by Mishin et al. [10]. Table 1 gives the lattice parameter, cohesive energy, elastic constants and stacking fault energy for each of the potentials. The three Ni potentials used in the simulations give almost identical elastic constants, cohesive energies and lattice parameters (close to experimental values), whereas the stacking fault energy given by the potentials varied from 60 to 120 mJ m^{-2}. The Shockley partial spacing width d for the screw dislocation varies from $d/\mathbf{b} = 5$ for potential vnih to $d/\mathbf{b} = 8$ for potential vni. The Angelo potential gives a $d/\mathbf{b}$ ratio of approximately six. This allows determination of the cross-slip activation energy as a function of $d/\mathbf{b}$ ratio. Since the experimentally determined stacking fault energy of Ni is close to 120 mJ m^{-2}, the results for cross-slip activation energy from potential vnih should be representative of Ni. The EAM potential developed for Cu by Mishin et al. [10] gives lattice parameter, cohesive energy, elastic constants and stacking fault energy values which are very near the experimental values and cross-slip activation energy results from this potential should be representative of Cu. The Mishin potential gives a $d/\mathbf{b}$ ratio of 6 for Cu. This is identical to the $d/\mathbf{b}$ ratio given for Cu by the potential Rasmussen et al. [11] used in their simulations of the Escaig process for cross-slip in bulk.

Table 1
Lattice parameter (a_0), cohesive energy (E_c), elastic constants (C_{11}, C_{12} and C_{44}) and stacking fault energy (γ) given by the three EAM potentials for Ni Angelo, vni and vnih, as well as the Mishin EAM potential for Cu.

Property	vni	vnih	Angelo	Mishin
a_0 (nm)	0.3518	0.3526	0.3520	0.3615
C_{11} (N m^{-2})	2.44×10^{11}	2.44×10^{11}	2.46×10^{11}	1.70×10^{11}
C_{12} (N m^{-2})	1.49×10^{11}	1.49×10^{11}	1.47×10^{11}	1.23×10^{11}
C_{44} (N m^{-2})	1.25×10^{11}	1.19×10^{11}	1.25×10^{11}	0.76×10^{11}
E_c (eV)	−4.43	−4.43	−4.45	−3.54
γ (J m^{-2})	00.059	0.119	0.089	0.044

2.2. Depiction of core structures

In order to illustrate the relaxed screw dislocation geometries we took advantage of the increase in atomic energy produced by the strain field of the partial dislocations. By plotting the atoms having assigned energies within LAAMPs of greater than −4.42 or −4.40 eV (Ni) or −3.52 eV (Cu) (the energy of atoms in the stacking fault region) the Shockley partial dislocation cores can be imaged easily, even for these large simulation cells. In order to illustrate the cross-slipped segment products of the screw dislocation the positions are shown in a [1 1 1] as well as a [1 1 $\bar{2}$] projection (viewed directions). For the [1 1 $\bar{2}$] projection segments spread on the initial (1 1 1) plane appear as a single line and cross-slipped segments (i.e. on a (1 1 $\bar{1}$) plane) appear as a pair of partials separated by a stacking fault.

3. Review of atomistic core structures for the 120° intersection

Figs. 2–4 depict the [1 1 1] and [1 1 $\bar{2}$] projections (i.e. the x–y and x–z planes) of the various core structures obtained for the screw dislocation–120° dislocation intersection, discussed in Rao et al. [6], obtained using the Angelo EAM potential for Ni. The starting configurations and boundary conditions were discussed in detail in our previous paper [6]. Fig. 2 illustrates a screw dislocation fully on the glide (1 1 1) plane and constricted (i.e. Stroh constrictions [12]) at both the intersections around one of the Shockley partials of the 120° 1/2[$\bar{1}$ 0 1] dislocation residing on the (1 $\bar{1}$ 1) plane. Fig. 3 depicts two Lomer–Cottrell lock configurations (LC1 and LC2) in the [1 1 1] and [1 1 $\bar{2}$] projections obtained for the screw dislocation–120° dislocation intersection. After relaxation the screw dislocation fully resides on the cross-slip (1 1 $\bar{1}$) plane (Fig. 3a and b). In Fig. 3b, as

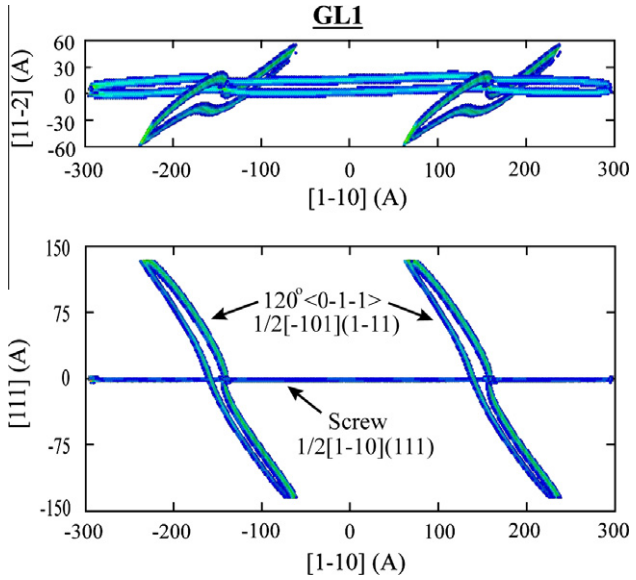

Fig. 2. [1 1 1] (x–y plane) and [1 1 $\bar{2}$] (x–z plane) projections of the core structure (GL1) for a screw–120° intersection in fcc Ni obtained from atomistic simulations using the Angelo EAM potential. Atoms having an energy greater than the energy at a stacking fault are plotted and correspond to the cores of Shockley partial dislocations.

in Fig. 2, the screw dislocation is constricted at both the intersections around one of the Shockley partials of the 120° 1/2[$\bar{1}$ 0 1] dislocation residing on the (1 $\bar{1}$ 1) plane. In Fig. 3a the a/6[1 $\bar{2}$ $\bar{1}$] Shockley partial of the screw dislocation combines with the a/6[$\bar{1}$ 1 2] Shockley partial of the 120° dislocation to form an extended node resulting in a short segment having a Burgers vector of the type 1/6[0 $\bar{1}$ 1] (e.g. a Lomer–Cottrell barrier). At the other end of the Lomer–Cottrell barrier, the screw dislocation is constricted to form one half of a Stroh constriction. Fig. 4 shows the [1 1 1] and [1 1 $\bar{2}$] projections for two core structures identified as partially cross-slipped locks (PCS1 and PCS2) obtained for the screw dislocation–120° dislocation intersection. In both cases the screw dislocation is partially on the glide (1 1 1) plane and partially on the cross-slip (1 1 $\bar{1}$) plane. In Fig. 4a, as in Fig. 2, the screw dislocation is constricted at both the intersections (negative constrictions [9,11]) around one of the Shockley partials of the 120° 1/2[$\bar{1}$ 0 1] dislocation residing on the (1 $\bar{1}$ 1) plane. Since the core is in the partially cross-slipped state, a companion positive constriction [9,11] forms between the intersections. In Fig. 4b, as in Fig. 3a, the a/6[1 $\bar{2}$ $\bar{1}$] Shockley partial of the screw dislocation combines with the a/6[$\bar{1}$ 1 2] Shockley partial of the 120° dislocation to form an extended node resulting in a short segment having a Burgers vector of type 1/6[0 $\bar{1}$ 1] (e.g. a Lomer–Cottrell barrier). At the other end of the Lomer–Cottrell barrier the screw dislocation is constricted to form one half of a negative constriction and is cross-slipped onto the glide (1 1 1) plane. Since the core is in the partially cross-slipped state, a companion full positive constriction forms between the intersections [9,11].

Fig. 5 depicts the [1 1 1] and [1 1 $\bar{2}$] projections (i.e. the x–y and x–z planes) of two of the core structures obtained for the screw dislocation–120° dislocation intersection, obtained using the Mishin EAM potential for Cu. The core structure shown in Fig. 5b for Cu is very similar to the core structure shown in Fig. 2 for Ni, with the screw dislocation fully on the glide (1 1 1) plane GL1 and the core structure shown in Fig. 5a for Cu is very similar to the core structure shown in Fig. 4a for Ni, with the screw dislocation partially on the glide (1 1 1) plane and partially on the cross-slip (1 1 $\bar{1}$) plane PCS1.

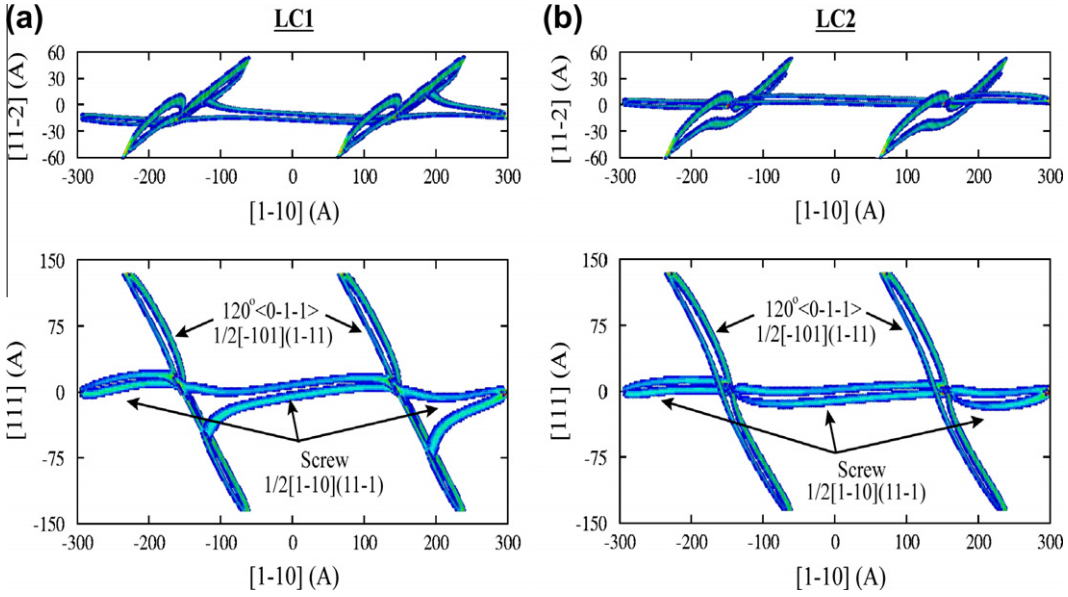

Fig. 3. [1 1 1] (x–y plane) and [1 1 $\bar{2}$] (x–z plane) projections of the core structures (LC1 and LC2) for a screw–120° intersection in fcc Ni from atomistic simulations using the Angelo EAM potential.

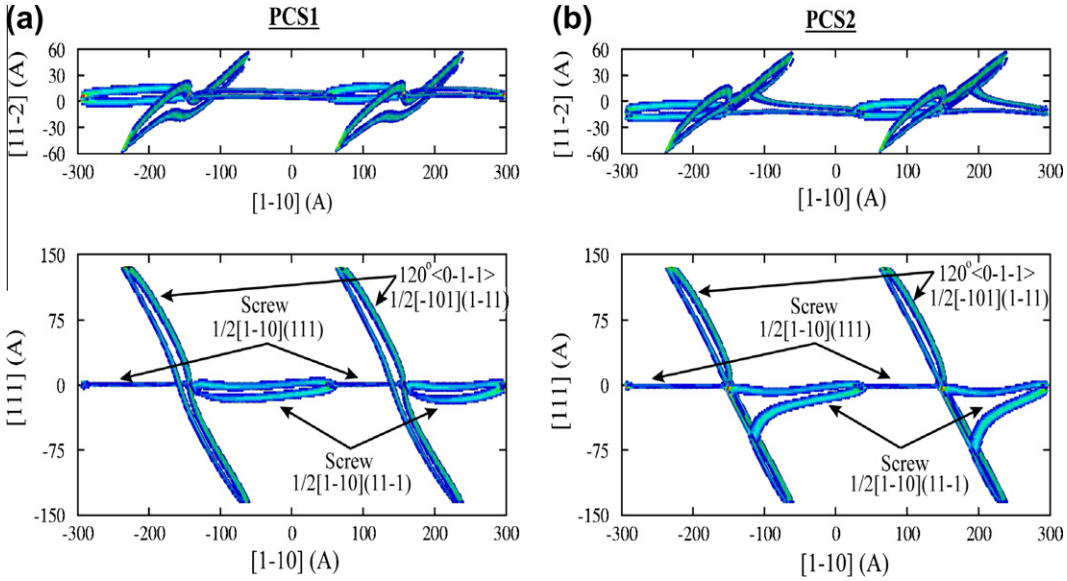

Fig. 4. [1 1 1] (x–y plane) and [1 1 $\bar{2}$] (x–z plane) projections of the core structures (PCS1 and PCS2) for a screw–120° intersection in fcc Ni from atomistic simulations using the Angelo EAM potential.

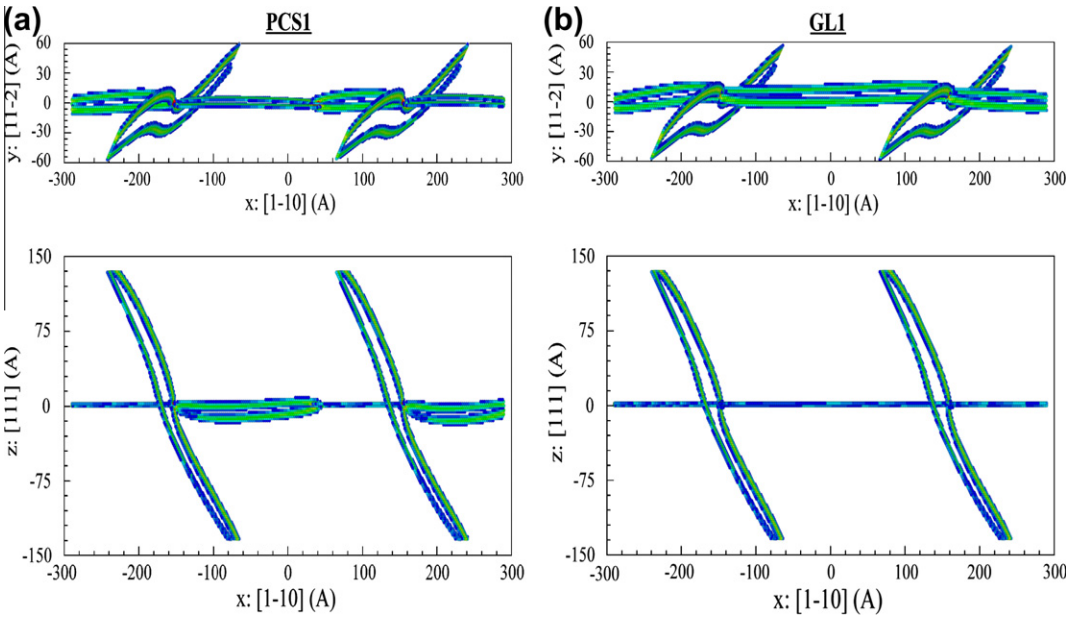

Fig. 5. [1 1 1] (x–y plane) and [1 1 $\bar{2}$] (x–z plane) projections of two of the core structures for a screw–120° intersection in fcc Cu from atomistic simulations using the Mishin EAM potential.

3.1. Schematic description of the energy well

Fig. 6 gives a schematic plot of the energy of the screw dislocation configuration at the intersection as a function of the length of screw dislocation cross-slipped onto the cross-slip plane in between the 120° intersecting dislocations. Previous molecular statics simulation results [6] showed that there are local minima in the energy curve when: the screw dislocation length on the cross-slip plane is zero (fully glide state), the entire screw dislocation length is on the cross-slip plane (fully cross-slipped state) and when approximately half the screw dislocation length between the intersections is on the cross-slip plane (partial cross-slip state). Two local maxima are expected for the energy versus state curve, in between the fully glide and partial cross-slip states and the fully cross-slip and partial cross-slip states. Starting from the partial cross-slip state, application of increasing Escaig stresses to the configuration were used to drive the screw dislocation up the energy well until a point of inflexion (e.g. the first derivative of the energy curve and the stress was maximum). For stresses slightly above the point of inflexion in the energy curve

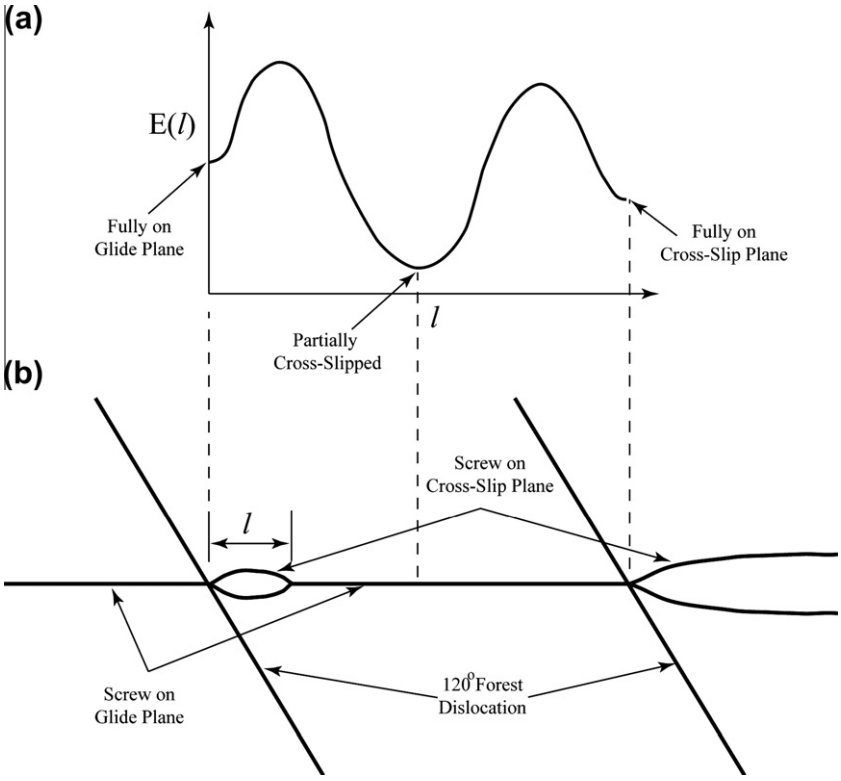

Fig. 6. (a) A schematic plot of the energy profile of the screw dislocation configuration as a function of the length of the screw dislocation on the cross-slip plane in between the forest dislocation intersections. (b) A schematic sketch of the $[1\,1\,\bar{2}]$ projection of the screw dislocation configuration in between forest dislocation intersections under applied Escaig stresses.

the screw dislocation will collapse to either the fully glide or fully cross-slip state. The work done by the Escaig stresses up to the inflexion point gives the energy required for the screw dislocation to transfer from the partially cross-slipped state to the fully glide plane or fully cross-slip plane states. The maximum Escaig stresses under which the partial cross-slipped state is stable are given by the maximum of the first derivative of this energy profile.

The following procedure was used to determine the local maxima, i.e. the activated state, for transforming the screw dislocation from fully glide plane or fully cross-slip plane states to the partially cross-slipped state in the energy curve. Partially cross-slipped states under Escaig stresses slightly above the maximum of the first derivative of the energy curve were relaxed and stopped at different points along the energy curve. The Escaig stresses were relaxed back to zero. Depending on the initial value of the Escaig stress and the position on the activation surface, under zero stress the screw dislocation configuration will collapse to one of the three possible minimum energy states: partially cross-slipped, fully glide plane or fully cross-slipped. The point at which the screw dislocation transitions from relaxing to the partially cross-slipped state to relaxing to the fully glide plane or fully cross-slipped plane states is identified as the maxima in the energy curve or the activated state for cross-slip. The energy of this configuration relative to the fully glide plane or fully cross-slip plane states was evaluated by using two relaxation techniques from the activated configuration, which are described in Section 3.4.

3.2. Behavior of cores PCS1 and PCS2 under stress

Fig. 7 gives the relaxed core structures in the $[1\,1\,\bar{2}]$ projection for the screw–120° intersection (core structure PCS1) for uniform compressive applied stresses of 250, 500, 750, 1000, 1100 and 1150 MPa along the [1 1 1] direction, obtained using the Angelo EAM potential. For the 1150 MPa case an additional increment of 50 MPa compressive stress was applied on the relaxed 1100 MPa compressive stress configuration. With increasing compressive applied stress the amount of cross-slipped screw segment in between the two intersecting 120° dislocations monotonically increased until a stress of 1100 MPa was reached. When the compressive applied stress was slightly increased from 1100 to 1150 MPa the screw dislocation in between the intersections suddenly collapsed to core structure LC2, fully residing on the cross-slip $(1\,1\,\bar{1})$ plane. For compressive applied stresses the effective stacking fault energy on the cross-slip $(1\,1\,\bar{1})$ plane decreased by an amount equal to $\tau_e b_e$, where $\tau_e = S\sigma_c$, S is the Schmidt factor acting on the edge component of the Shockley partials on the cross-slip $(1\,1\,\bar{1})$ plane, σ_c is the applied compressive stress along the [1 1 1] direction and b_e is the magnitude of the edge component = 0.071 nm.

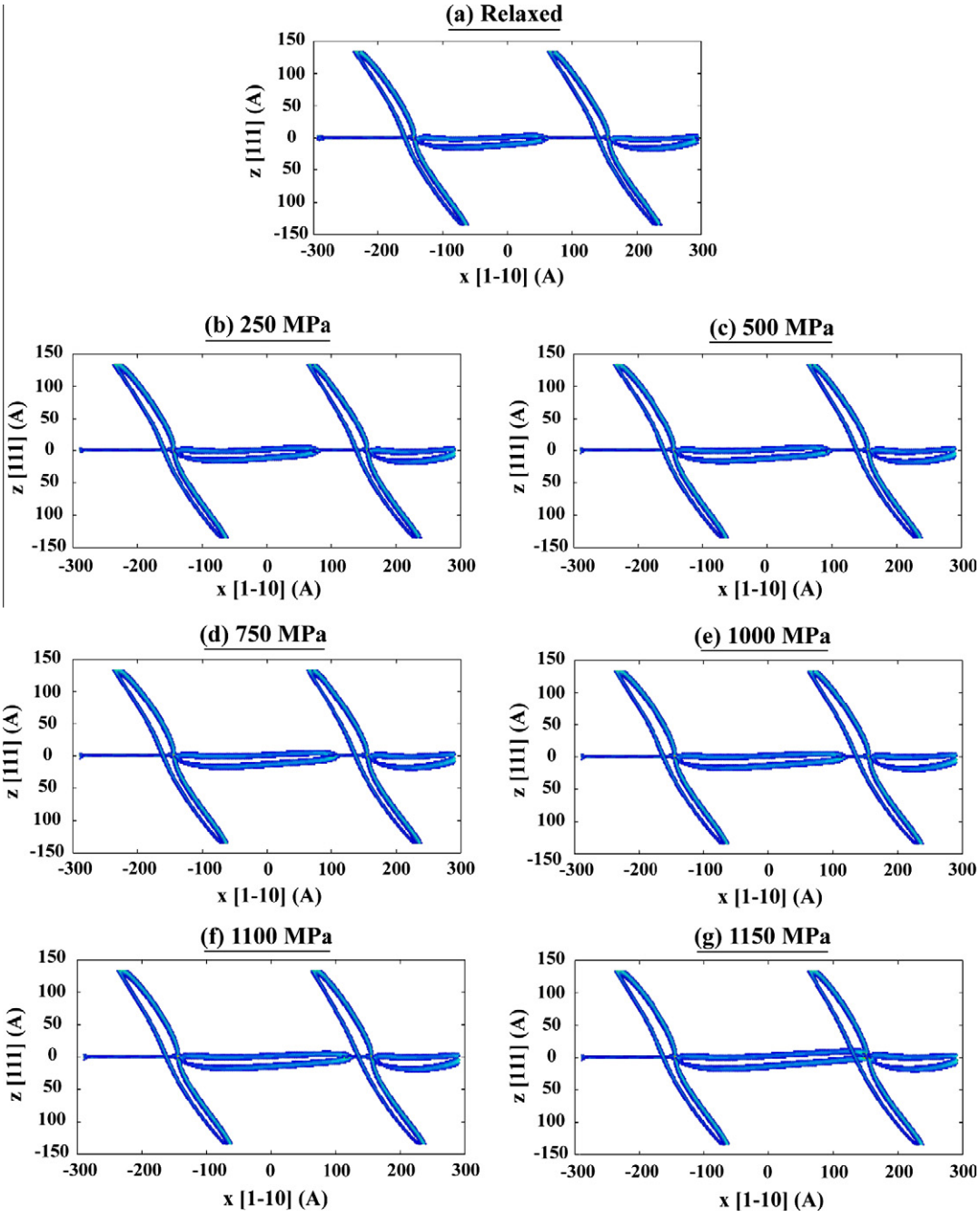

Fig. 7. The [1 1 $\bar{2}$] projection of the equilibrium configurations of the partially cross-slipped core structure, PCS1, under uniform applied compressive stresses of 0, 250, 500, 750, 1000, 1100 and 1150 MPa applied along the [1 1 1] direction, obtained using the Angelo EAM potential for Ni.

Similar behavior was observed for uniform tensile applied stresses along the [1 1 1] direction. In this case, the amount of cross-slipped segment in between the two intersecting 120° dislocations montonically decreased until a stress of 1000 MPa was reached. When the tensile applied stress was slightly increased from 1000 to 1050 MPa the screw dislocation in between the intersections suddenly relaxed to core structure GL1, fully residing on the glide (1 1 1) plane. For tensile applied stresses the effective stacking fault energy on the cross-slip (1 1 $\bar{1}$) plane increased by an amount equal to $\tau_e b_e$, where $\tau_e = S\sigma_t$ and σ_t is the applied tensile stress along the [1 1 1] direction.

Similar behavior was observed for core structure PCS2. In this case, when the applied stress was compressive core structure PCS2 relaxed to core structure LC1 when the compressive stress was increased from 650 to 700 MPa. Similarly, for tensile applied stresses core structure PCS2 relaxed to core structure GL1 when the applied tensile stress was increased from 1150 to 1200 MPa.

3.3. Analysis of cores PCS1 and PCS2 under applied stresses

Fig. 8a and b illustrates the change in length of the cross-slipped segment in between the two intersecting

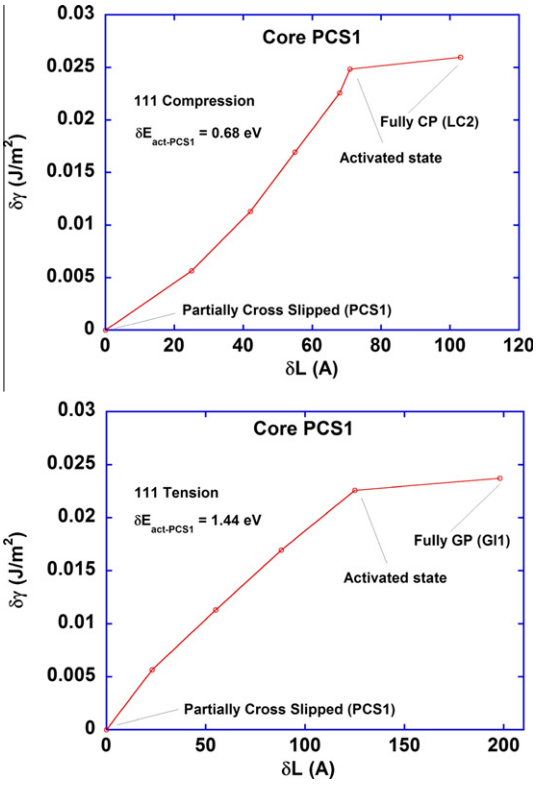

Fig. 8. A plot of the increase or decrease in length of the cross-slipped segment in between the two intersecting 120° dislocations (x-axis) versus the decrease or increase in effective stacking fault energy (y-axis) due to the applied compressive or tensile stresses along the [1 1 1] direction for initial core structure PCS1 obtained using the Angelo EAM potential for Ni. The activation barrier for the transition of the dislocation from the partially-cross-slipped state (PCS1) to the either the fully cross-slipped plane state (LC2) or the fully glide plane state (GL1) is also indicated.

120° dislocations (x-axis) versus the change in effective stacking fault energy (y-axis) due to the applied compressive or tensile stresses along the [1 1 1] direction for initial core structure PCS1 obtained using the Angelo EAM potential. Fig. 8a and b clearly shows that for a certain critical increase or decrease in stacking fault energy, δ_γ, the core structure for the intersection collapsed to either LC2, fully residing on the cross-slip plane (compressive stress), or GL1, fully residing on the glide plane (tensile stress). The work done by the applied stresses up to the critical point is given by the area under the curve up to the critical point multiplied by the Shockley partial spacing (estimated to be 6**b**, where **b** is the magnitude of the Burgers vector of the screw dislocation [9]) and is equal to the energy difference between the activated states and the partially cross-slipped state PCS1, $\delta E_{\text{act–PCS1}}$. This is determined to be 0.68 eV for the activated state on the compressive side and 1.44 eV for the activated state on the tensile side. The Escaig stresses required to transform the dislocation from the partially cross-slipped state (PCS1) to the fully glide plane state (on the tensile side GL1) is 314 MPa and to the fully cross-slipped state (LC2) is 346 MPa.

Similar analysis was performed for core structure PCS2.The Escaig stresses required to transform the dislocation from the partially cross-slipped state (PCS2) to the fully glide plane state (on the tensile side GL1) is 361 MPa and to the fully cross-slipped state (on the compressive side LC1) is 204 MPa.

3.4. Determination of cross-slip activation energy

To determine the activation energy for cross-slip from the fully glide plane state (GL1) to the partially cross-slipped state (PCS1) the simulation having 1050 MPa tensile stress applied to the partially cross-slipped state PCS1 was stopped after varying amounts of relaxation and the applied stress relaxed back to zero. Conjugate gradient minimization after the stress was relaxed back to zero indicated whether the core relaxed to the partially cross-slipped state (PCS1) or the fully glide plane state (GL1). The configuration at which the relaxation transitions from relaxing to PCS1 to relaxing to GL1, was taken to be the activated state for cross-slip from GL1 to PCS1. Fig. 9 gives the structure of the activated state in the [1 1 $\bar{2}$] projection for the screw–120° intersection (core structure PCS1) obtained

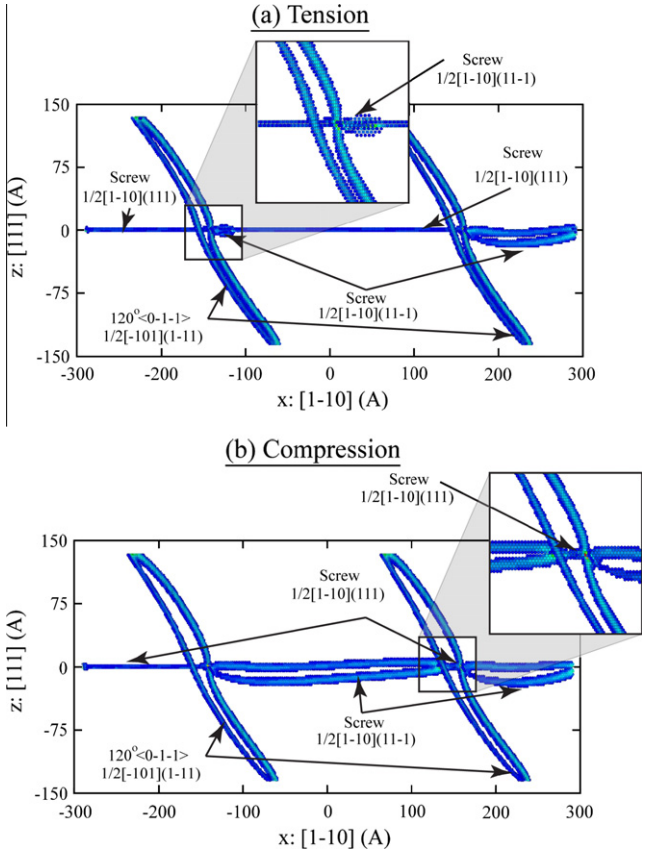

Fig. 9. The [1 1 $\bar{2}$] projection of the structure of the activated configuration for transition of the screw dislocation from (a) state GL1 to PCS1 (tensile side) and (b) state LC2 to state PCS1 (compressive side) obtained using the Angelo EAM potential for Ni. The x-axis is along the [1 $\bar{1}$ 0] direction and the y-axis is along the [1 1 1] direction. The square boxes indicate regions shown at higher magnification in the insets.

using the Angelo potential, which gives a stacking fault energy of 90 mJ m^{-2}. Fig. 9a shows that in the activated configuration a small portion of the screw dislocation near the intersection, of length $\sim 1.5d$, resides on the cross-slip plane. The attractive interaction between the negative and the positive constrictions becomes zero at a separation distance of $1.5d$, beyond which it becomes repulsive, in the presence of an intersecting dislocation. This behavior is significantly different from the typical Escaig process for cross-slip, where the attractive interaction between the constrictions only becomes zero at an infinite separation distance [2–4].

A similar analysis was performed to determine the activation energy for cross-slip from the fully cross-slip plane state (LC2) to the partially cross-slipped state (PCS1). In this case the simulation having a 1150 MPa compressive stress applied to the partially cross-slipped state PCS1 was stopped after varying amounts of relaxation and the applied stress relaxed back to zero. Conjugate gradient minimization after the stress was relaxed back to zero indicated whether the core relaxed to the partially cross-slipped state (PCS1) or the fully cross-slip plane state (LC2). The configuration at which the relaxation transitioned from relaxing to PCS1 to collapsing to LC2 was taken to be the activated state for cross-slip from LC2 to PCS1. Fig. 9b shows that in the activated configuration a small portion of the screw dislocation near the intersection, of length $\sim d$, resided on the glide plane. The attractive interaction between the negative and the positive constrictions became zero at a separation distance of d, beyond which it became repulsive, in the presence of an intersecting dislocation. Again, such behavior is significantly different from the standard Escaig process.

A similar analysis was performed on the partially cross-slipped state (PCS1) obtained using the Mishin potential for Cu, and the activated states obtained using this potential on both the tensile and compressive sides were very similar to the activated configurations obtained using the Angelo potential for Ni.

The activation energy for cross-slip from state GL1 to state PCS1, $\delta E_{\mathrm{GL1-PCS1}}$ was determined using two different relaxation techniques from the identified activated configuration. In the first technique the energy was determined for relaxation from the activated state to state GL1 under an applied tensile stress of 1050 MPa (Angelo potential for Ni) along the [1 1 1] direction. This energy was corrected for two factors to obtain the activation energy for cross-slip: (a) work done by the applied Escaig stresses in collapsing the activated configuration (of the order of 0.2 eV); (b) the increase in energy of the activated configuration due the applied Escaig stresses (of the order of 0.4 eV). For the second technique the activated state was relaxed to state GL1 having zero applied stress, with and without atoms within a cube of size 1.2 nm centered at the positive constriction of the activated state fixed. The difference in relaxation energies between the two types of simulations was taken to be the activation energy for cross-slip from GL1 to PCS1. The results for the cross-slip activation energy obtained using these two techniques of relaxation were within 0.2 eV of each other and were taken to be representative of the error in the determination of the activation energy for cross-slip using this procedure. The activation energy for cross-slip from state GL1 to state PCS1, $\delta E_{\mathrm{GL1-PCS1}}$, was also determined when the separation distance between the two intersecting forest dislocations was 90 nm, as opposed to 30 nm, and the cross-slip activation energy was found to be independent of the separation distance used in the simulations.

Similar simulations and analyses were performed to determine the activation energy for cross-slip from GL1 to PCS1 using two other Ni EAM potentials, vni and vnih. Also, similar simulations and analyses were performed to determine the activation energy for cross-slip from the fully cross-slip plane state (LC2) to the partially cross-slipped state (PCS1) using all three EAM potentials, $\delta E_{\mathrm{LC2-PCS1}}$. For these cases the two techniques of relaxation described before for determining the cross-slip activation energy gave values that differed by less than 0.1 eV.

Fig. 10 is a plot of the cross-slip activation energies for cross-slip from state GL1 to state PCS1 as well as from state LC2 to state PCS1, obtained using the three Ni EAM potentials, versus the parameter $(d/\mathbf{b})[\ln(\sqrt{3}d/\mathbf{b})]^{1/2}$ given by the potentials. Also plotted in Fig. 10 are the corresponding values for the cross-slip activation energy determined from simulations of the Escaig process as well as the cross-slip activation energies obtained for the case of a single intersecting dislocation, as opposed to two, with the Angelo Ni potential [9]. Fig. 10 clearly shows that the cross-slip activation energy is linearly proportional to $(d/\mathbf{b})[\ln(\sqrt{3}d/\mathbf{b})]^{1/2}$ both at the intersection and for the Escaig type process. The cross-slip activation energy (from GL1 to PCS1) values near the intersection were a factor of three lower than that for the Escaig process. Also, the cross-slip

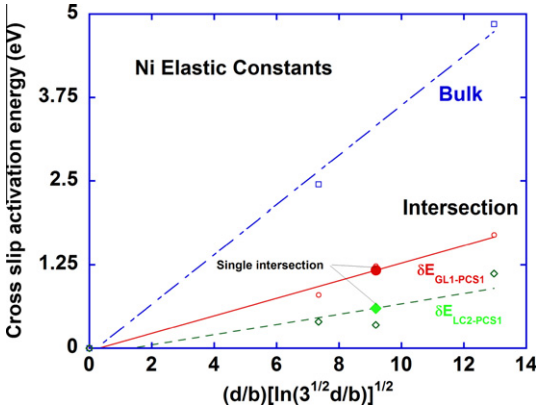

Fig. 10. A plot of the activation energy for cross-slip from state GL1 to state PCS1 ($\delta E_{\mathrm{GL1-PCS1}}$) as well as from state LC2 to state PCS1 ($\delta E_{\mathrm{LC2-PCS1}}$) in Ni as a function of the parameter $d/\mathbf{b}[\ln(\sqrt{3}d/\mathbf{b})]^{1/2}$ given by the EAM potentials Angelo, vni and vnih. Also shown are the corresponding cross-slip activation energy values for the Escaig process operating in a bulk crystal [9] as well as cross-slip activation energy values obtained for the case of a single intersecting dislocation, as opposed to two, with the Angelo potential.

activation energy from the fully cross-slip plane state (LC2) to the partially cross-slipped state (PCS1) was approximately a factor of five lower than that for the Escaig process. The $\delta E_{\mathrm{LC2\text{–}PCS1}}$ value can be identified, by symmetry, as the cross-slip activation energy from the fully glide plane state to the partially cross-slipped state at a 120° screw dislocation intersection, where the intersecting forest dislocation has a $1/2\langle 0\,1\,1\rangle$ Burgers vector $\langle 1\,0\,\bar{1}\rangle$, line direction and resides on the $(1\,\bar{1}\,1)$ plane. This suggests that the cross-slip activation energy near an intersection is strongly dependent on the Burgers vector of the intersecting dislocation and could be a factor of five lower than that usually considered. Fig. 10 also shows that the presence of a second intersecting dislocation has very little effect on the calculated cross-slip activation energies at the intersections.

The activation volume for the cross-slip process with respect to applied Escaig stresses is given by the area of the cross-slipped portion of the screw character dislocation in the activated state (Fig. 9) multiplied by the magnitude of the edge component of the Burgers vector of the Shockley partials. From the simulations values for this parameter ranged from 10 to $20\mathbf{b}^3$ for cross-slip at screw dislocation intersections.

Similarly, the cross-slip activation energies at the 120° intersection, $\delta E_{\mathrm{GL1\text{–}PCS1}}$ as well as $\delta E_{\mathrm{LC2\text{–}PCS1}}$, were determined using the Mishin potential for Cu. These values were determined to be 1.13 and 0.65 eV, respectively. These values are factors of 2–3 lower than that for the Escaig process (1.7 eV) (unpublished calculations of cross-slip activation energy via the Escaig process in bulk for Cu using the Mishin potential by SI Rao (positive constriction 3.0 eV, negative constriction −1.3 eV)). The values of 1.13 and 0.65 eV determined for the cross-slip activation energies at the 120° intersection are in reasonable accord with the experimentally determined value for cross-slip activation energy in Cu, 1.15 eV [13]. This suggests that cross-slip preferentially occurs at selected screw dislocation intersections in fcc materials.

4. Discussion

This work has shown that the activation energy for nucleation of cross-slip in the bulk of an fcc metal can be sufficiently small to enable profuse cross-slip through thermal activation under multi-slip conditions. Further, this work provides a methodology to obtain the variation in nucleation barrier with type of slip system interaction within a given system. These calculations can be directly used in higher level mesoscale simulations where cross-slip statistics can be accounted for. The results are likely to permit improved simulations of metallic behavior, such as work hardening and fatigue, that have not been possible without ad hoc assumptions about cross-slip. We include below a few remarks on our results, including limitations.

The results clearly show that cross-slip nucleation at screw dislocations intersecting forest dislocations exhibits an activation energy that is a factor of 2–5 lower than that for the Escaig mechanism. It is worth noting that the probability of dislocation intersections is relatively large as compared with other mechanisms of obstacle-induced cross-slip, like cross-slip at screw dipoles, jogs and surfaces [14–16]. Further, cross-slip at screw dipoles, jogs and surfaces is athermal only under specific conditions [14–16]. The current results rationalize the experimentally observed profuse nature of cross-slip in fcc crystals in a more satisfactory manner than the current models of thermally activated cross-slip that require high stress to provide a self-consistent explanation.

Acknowledging a limitation of this work, we note that since a molecular statics technique has been used, the cross-slip activation energy values reported in this manuscript are expected to be upper bounds. A more sophisticated molecular dynamics reaction pathway technique [17] might provide more accurate values for the activation energies of cross-slip near forest dislocation intersections.

The new cross-slip nucleation model has a variety of implications for crystal plasticity in fcc materials. For example, within the present mechanism the frequency of cross-slip should scale with the forest dislocation density, i.e. multiplication rate proportional to ρ_f. The growth of such nuclei should depend upon the relative magnitude of local stresses on the glide plane and the cross-slip plane at the partially cross-slipped screw–dislocation intersection region. Such behavior of the partially cross-slipped core under different modes of applied stress could be studied using atomistic simulations as well as dislocation dynamics simulations. Similar activation analyses using atomistic simulations must be performed for other intersections (varying the line direction of the intersecting dislocation) on the $(1\,\bar{1}\,1)$ plane that form glide, Lomer–Cottrell or Hirth locks to determine the dependence of the activation energy for cross-slip on the line direction as well as the Burgers vector of the intersecting forest dislocation. The intersection mechanism of cross-slip nucleation should also be implemented in 3D dislocation dynamics simulations as an alternative to Escaig's model for fcc materials. Finally, it would be instructive to revisit the Bonneville and Escaig experimental results on cross-slip in fcc Cu in the light of the new intersection mechanism for cross-slip nucleation [1,13].

According to Washburn [18], double intersection cross-slip, where the segment that has been pulled into the cross-slip plane soon encounters another attractive intersection that brings it back onto another primary glide plane, provides a reasonable mechanism for dislocation multiplication and the growth of slip bands at low temperatures. Naturally, such a mechanistic process must be demonstrated via modern simulation methods. Also, classical theories of strain hardening assume that dislocation storage in Stage II of single-crystal fcc materials is a result of junction formation [19] or two-dimensional (2D) concave loop formation [20] as the gliding dislocation traverses through an array of forest dislocation obstacles on its glide plane. However, one of the major problems in classical strain hardening models is to explain how the generation of a

3D network of stored dislocations occurs as a consequence of 2D glide [20]. We note that the intersection cross-slip nucleation mechanism for dislocation storage may provide a convenient mechanism of generating a 3D network of stored dislocations from 2D glide.

Finally, the anomalous flow behavior of intermetallics (i.e. Ni_3Al) has thus far been modeled using core transformations that require thermal activation. Here again, the key issue has been that constriction energies are prohibitively high [2,3,21]. The possibility of core transformation in the presence of interaction with other dislocations provides a novel mechanism to consider and explore in rationalizing the flow anomaly of these types of materials.

5. Summary

Atomistic simulations were conducted to identify the saddle point configuration and thus the activation energy for cross-slip of a screw dislocation in the presence of a pair of forest dislocations. The approach involved the use of external stress along [1 1 1] to vary the segment length for a partially cross-slipped $1/2[1\,\bar{1}\,0]$ screw dislocation intersecting a pair of 120° $1/2[\bar{1}\,0\,1]$ Burgers vector, $\langle 0\,\bar{1}\,\bar{1}\rangle$ line direction dislocations residing on the $(1\,\bar{1}\,1)$ plane. The simulations in this work show that the nucleation of cross-slip at dislocation–dislocation interactions is significantly more probable than that for the Escaig process, having an activation barrier that is a factor of 2–5 lower. Further, this work shows that atomistic simulations can be used to identify types of interactions that result in cross-slip and these results in turn may be used in higher level mesoscale simulations.

Summarizing the results, equilibrium partially cross-slipped core structures under applied compressive or tensile stresses along the [1 1 1] direction were determined using atomistic simulations. Beyond a critical stress the equilibrium configurations relax to a core structure that is either fully on the glide plane for tensile stresses or fully on the cross-slip plane for compressive stresses.

The activation barrier for cross-slip from the fully glide plane state (GL1) to the partially cross-slipped state (PCS1), $\delta E_{\mathrm{GL1–PCS1}}$, at these intersections was determined to be a factor of three lower than that for the conventional Escaig-based mechanism. While the new cross-slip mechanism has a lower activation energy it has the same linear relationship to $(d/\mathbf{b})[\ln(\sqrt{3}d/\mathbf{b})]^{1/2}$ as the Escaig process.

The activation barrier for cross-slip from the fully cross-slip plane state (LC2) to the partially cross-slipped state (PCS1), δE_{LC2}, at these intersections was determined to be approximately a factor of five lower than for the Escaig process. These $\delta E_{\mathrm{LC2–PCS1}}$ values were identified, by symmetry, as the activation barrier for cross-slip from the fully glide plane state to the partially cross-slipped state at a 120° screw dislocation intersection, where the intersecting dislocation has a $1/2\langle 0\,1\,1\rangle$ Burgers vector $\langle 1\,0\,\bar{1}\rangle$, line direction and resides on the $(1\,\bar{1}\,1)$ plane.

Cross-slip activation energy values near forest dislocation intersections in fcc Cu were determined to be 1.13 and 0.65 eV. Though anticipated to be upper bound values, these values are in reasonable accord with the experimentally determined value for cross-slip activation energy in Cu, 1.15 eV [13]. This suggests that cross-slip preferentially occurs at selected screw dislocation intersections in fcc materials.

Acknowledgements

The authors acknowledge use of the three-dimensional molecular dynamics code LAAMPS, which was developed at Sandia National Laboratory by Dr. Steve Plimpton and co-workers. This work was supported by the AFOSR under USAF Contract No. FA8650-04-D-5235, and by a grant of computer time from the DOD High Performance Computing Modernization Program at the Aeronautical Systems Center/Major Shared Resource Center. The work was performed at the US Air Force Research Laboratory, Materials and Manufacturing Directorate, Wright-Patterson Air Force Base.

References

[1] Bonneville J, Escaig B. Acta Metall 1979;27:1477.
[2] Escaig B. In: Rosenfield AR, Hahn GT, Bement AL, Jaffee RI, editors. Proceedings of the Battelle colloquium on dislocation dynamics. New York: McGraw-Hill; 1968. p. 655.
[3] Puschl W. Prog Mater Sci 2002;47:415.
[4] Caillard D, Martin JL. Thermally activated mechanisms in crystal plasticity. Amsterdam: Pergamon–Elsevier; 2003.
[5] Saada G. Mater Sci Eng 1991;A137:177.
[6] Rao S, Dimiduk DM, El-Awady J, Parthasarathy TA, Uchic MD, Woodward C. Philos Mag 2009;89(34):3351.
[7] Plimpton SJ. J Comput Phys 1995;117:1.
[8] Angelo JE, Moody NR, Baskes MI. Modell Simul Mater Sci Eng 1995;3:289.
[9] Rao S, Parthasarathy TA, Woodward C. Philos Mag A 1999;79:1167.
[10] Mishin Y, Mehl MJ, Papaconstantopoulos DA, Voter AF, Kress JD. Phys Rev B 2001;63:224106.
[11] Rasmussen T, Jacobsen KW, Leffers T, Pedersen DB. Phys Rev B 1997;56:2977.
[12] Stroh AN. Philos Mag 1959;3:625.
[13] Bonneville J, Escaig B, Martin JL. Acta Metall 1988;36:1989.
[14] Rao S, Dimiduk DM, Jaafar El-Awady, Parthasarathy TA, Uchic MD, Woodward C., submitted for publication.
[15] Brown LM. Philos Mag A 2002;82:1691.
[16] Vegge T, Jacobsen KW. J Phys Condens Matter 2002;14:2929.
[17] Pendurti S, Jun S, Lee I, Prasad V. Appl Phys Lett 2006;88:201908.
[18] Washburn J. Appl Phys Lett 1965;7:183.
[19] Devincre B, Hoc T, Kubin L. Science 2008;320:1745.
[20] Kocks UF, Mecking H. Prog Mater Sci 2003;48(3):102.
[21] Parthasarathy TA, Dimiduk D. Acta Mater 1996;44:2237.